Dynamical screening in K-shell photoionization

Jia-Ming Li

*Center of Theoretical Physics, Chinese Center of Advanced Science and Technology (World Laboratory),
and Institute of Physics, Academia Sinica, Beijing, China*

Ying-Jian Wu

Institute of Physics, Academia Sinica, Beijing, China

R. H. Pratt

Department of Physics and Astronomy, University of Pittsburgh, Pittsburgh, Pennsylvania 15260

Starting from the Hartree-Slater independent electron model, we perform configuration interaction (CI) calculations for both the initial state and the final state in atomic photoionization processes. Our CI K-shell photoionization cross section for Ne displays an enhancement near the threshold due to the dynamical screening effect of the K vacancy, which is in good agreement with experiments. Furthermore, the K-shell ratio function of the CI Ne K shell to the CI Ne$^+$ K-shell photoionization cross sections shows no oscillatory behavior, in contrast to the ratio in the Hartree-Slater independent electron calculation.

I. INTRODUCTION

There is a great deal of interest in photoionization processes because one can learn dynamical properties of the interactions, not only between the incident photon and the atomic electrons but also between the ejected electron and the residual atomic electrons. Historically, an independent particle approximation (IPA) such as the Hartree-Slater method provides a convenient method to calculate the photoionization cross sections and can also explain most of the nonhydrogenic features (e.g., atomic screening effects) in photoionization processes. General physical properties of photoionization cross sections for the neutral atoms in their ground states (i.e., oscillator strength density distribution) have been reviewed.[1,2] For example, IPA gives the main features of Cooper minima and delayed maxima in the photoionization cross sections,[1] although the exact quantitative description of these nonhydrogenic features sometimes requires more precise theoretical calculations beyond the IPA. Owing to recent developments in laser technology and fusion plasma research, there is also much interest in photoionization processes for excited atoms as well as ionized atoms. Some aspects of photoionization of such targets have now been investigated.[3-8] For example, since all photoionization cross sections behave similarly in shape for neutral and ionized atoms,[3,4,6] a subshell ratio function for an ion can be introduced as the ratio of the subshell ion photoionization cross section to that for the corresponding neutral atom;[6] such subshell ratio functions vary smoothly with photon energy and, in the high photon energy region, approach constants asymptotically, not only for the inner subshells but also for the outer subshells. However, in regions near thresholds, the subshell ratio functions, calculated from Hartree-Slater-type potentials with the Coulomb Latter tail, have oscillatory behaviors.[7-9] Such oscillatory behaviors are associated with a discontinuity in the derivative of the Hartree-Slater-type potential at the joining point of the Coulombic tail.[8,9] In addition, dynamical correlations also become important near the threshold regions. Thus to achieve a better understanding of photoionization near thresholds requires more precise theoretical calculation methods beyond the IPA methods.

There have been various theoretical approaches beyond the IPA for atomic photoionization, such as the configuration interaction (CI) method,[10-14] the R-matrix method,[15-18] the random-phase approximation,[19,20] the many-body perturbation method,[21,22] etc. Here we adopt the CI method, more specifically to calculate separately the initial-state atomic wave function by a superposition of the relevant configuration functions and the final-state wave functions by superpositions of the relevant configuration functions including the continua. Photoionization is then treated as a first-order perturbation process between the initial and the final states. This approach provides a clearer picture to elucidate the initial-state correlations, the final-state correlations, and the dynamical correlations linked by one photon absorption in the atomic photoionization processes. Here, we choose K-shell photoionization for the neutral Ne atom and the Ne$^+$ ion as an illustrative example. We start with the Hartree-Slater IPA method. In such a calculation the K-shell ratio function displays an oscillatory behavior near the threshold region. With the CI method we can take into account the residual interactions which have been omitted in the IPA method. Our calculated CI K-shell ratio function has no oscillation, as shown in Fig. 1. We also compare the CI K-shell photoionization cross section with the existing experimental data[23-25] for the neutral Ne atom. We have not taken into account the shakeup and the shakeoff channels (in which while a K-
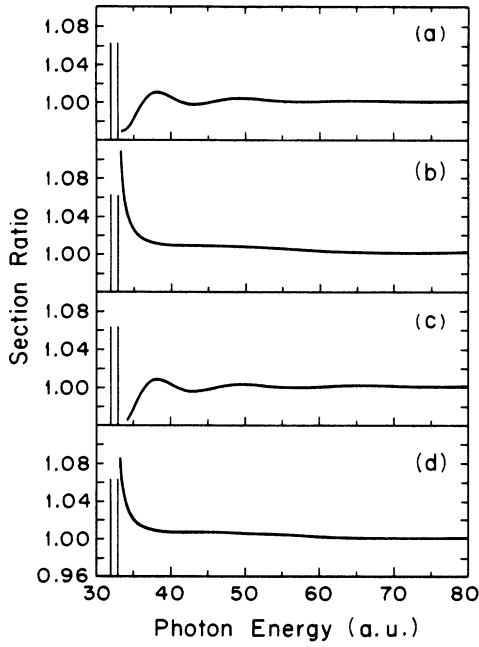
FIG. 1. K-shell ratio function of $\sigma(\text{Ne}^+)/\sigma(\text{Ne})$. (a) Hartree-Slater (HS) initial-state and HS final-state wave functions. (b) HS initial-state and CI final-state wave functions. (c) CI initial-state and HS final-state wave functions. (d) CI initial-state and CI final-state HS wave functions.
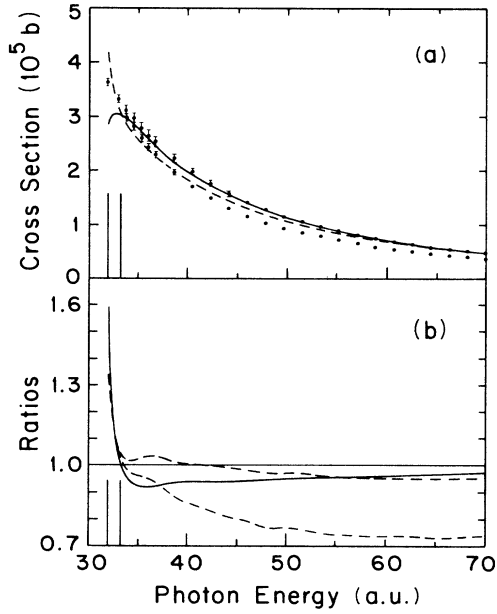

FIG. 2. K-shell photoionization cross section for the neutral Ne atom. (a) K-shell cross sections. Solid curve: Hartree-Slater result. Dashed curve: our CI total cross section. Points: experimental data (Refs. 23 and 24) (upper—K-shell total cross section; lower—K-shell partial cross section with Ne$^+$ in ground state). (b) Ratios of K-shell cross sections with respect to the Hartree-Slater cross section. Solid curve: our CI result. Dashed curve: experimental data (Refs. 23 and 24) (upper—K-shell total cross section, lower—K-shell partial cross section with Ne$^+$ and K vacancy). Solid vertical line: Ne K-shell threshold. Solid vertical line: Ne K-shell shakeup threshold.

shell electron is ionized, an outer-shell electron is also excited or ionized) in our present CI calculation, shown in Fig. 2, and our CI K-shell cross section is in best agreement with the experimental results below the shakeup threshold. This agreement demonstrates the importance of the dynamical screening effect on the photoelectron, due to the K vacancy in atomic K-shell photoionization. At the end of this paper we discuss the effects of the shakeup and the shakeoff channels in photoionization.

II. THEORETICAL METHOD AND RESULT

Since the interaction between the atomic system and the photon field is treated as a first-order perturbation process, we start with the total N-electron atomic Hamiltonian (in atomic units throughout):

$$H_a = \sum_i (P_i^2/2 - Z/r_i) + \sum_{i<j} 1/r_{ij} = H_{\text{HS}} + V , \qquad (1)$$

where H_{HS} is the Hartree-Slater Hamiltonian defined as

$$H_{\text{HS}} = \sum_i [P_i^2/2 + V_{\text{SCF}}(r_i)] . \qquad (2)$$

The Hartree-Slater potential V_{SCF} with the Coulomb Latter tail is readily calculated by a self-consistent method.[26,27] The residual interaction potential V, which has been omitted in the Hartree-Slater Hamiltonian, can then be defined as

$$V \equiv \sum_i -[V_{\text{SCF}}(r_i) + Z/r_i] + \sum_{i<j} 1/r_{ij} . \qquad (3)$$

Based on the Hartree-Slater potential V_{SCF}, one-electron wave functions including continuum wave functions can be conveniently calculated and form a complete orthonormal basis set. Antisymmetrized N-electron product-type configuration wave functions $\Phi_i(\Gamma,\gamma)$ with Γ and γ denoted as the quantum numbers (e.g., the angular momenta and their couplings) and the z-component projections form a complete orthonormal basis to describe the N-electron atomic system. The residual interaction matrix elements $\langle \Phi_i|V|\Phi_j \rangle$ can be conveniently calculated as one-electron matrix elements and two-electron matrix elements.[28]

We will now discuss briefly how to calculate the final-state and the initial-state wave functions (see Refs. 14 and 28 for the details). The initial-state wave function with $\Gamma = {}^1S$ for Ne or $\Gamma = {}^2P$ for Ne$^+$ is expressed as a superposition of the relevant configuration wave functions,

$$\Psi_I(\Gamma,\gamma) = \sum_i a_i \Phi_i(\Gamma,\gamma) . \qquad (4)$$

For the Ne atom, the ground-state configuration is $1s^2 2s^2 2p^6({}^1S)$. For the Ne$^+$ ion, the ground-state configuration is $1s^2 2s^2 2p^5({}^2P)$. The relevant configurations chosen in Eq. (4) consist of the ground-state configuration, one-electron excited bound-type configurations and two-electron excited bound-type configurations with $\Gamma = {}^1S$ for the Ne atom and $\Gamma = {}^2P$ for the Ne$^+$ ion, respectively. The superposition coefficients a_i are determined by diagonalizing the relevant Hamil-

tonian matrix.[28] In K-shell photoionization of the neutral Ne atom, the main configuration of the final state is $1s^2 2s^2 2p^6 (^2S)\epsilon P (^1P)$, with the configuration wave function denoted as $\Phi_\epsilon(\Gamma, \gamma)$, where $\Gamma = (^2S)^1P$. In K-shell photoionization for Ne$^+$, the main configuration of the final state is $1s^1 2s^2 2p^5(^1P$ or $^3P)\epsilon p (^2S, ^2P,$ or $^2D)$, with the configuration wave function denoted as $\Phi_\epsilon(\Gamma, \gamma)$, where $\Gamma = (^1P)^2S,$ $(^1P)^2P,$ $(^1P)^2D,$ $(^3P)^2S,$ $(^3P)^2P,$ and $(^3P)^2D$, respectively. In our present one-channel CI calculation (e.g., six separate calculations for the Ne$^+$ final states), the final-state wave functions are then expressed as[1,10-14]

$$\Psi_\epsilon(\Gamma, \gamma) = \int a_{\epsilon'}^\epsilon \Phi_{\epsilon'}(\Gamma, \gamma) d\epsilon' ,$$ (5)

where the integration also includes a sum over discrete configuration wave functions. Although the continuum configuration wave functions adopted are antisymmetrized product-type wave functions of the residual frozen-core configuration wave function ($N-1$ electrons) and the photoelectron wave function (one electron), the major part of the residual interactions due to the K vacancy (regarded as dynamical screening) should be taken into account. Of course, the residual interactions due to more delicate core relaxations, such as shakeup and shakeoff, have been completely ignored in our present calculation. Thus we anticipate our present one-channel calculations should best simulate the physical K-shell photoionization process below the core shakeup threshold. Further discussion on the implication of the residual frozen core will be given later.

Now, we return to the calculations of the superposition coefficients, which can be expressed as[1,10-14]

$$a_{\epsilon'}^\epsilon = \left[\frac{P}{\epsilon - \epsilon'} K_{\epsilon'\epsilon} + \delta(\epsilon - \epsilon') \right] B_\epsilon ,$$ (6)

where the matrix $K_{\epsilon'\epsilon}$ satisfies the Lippmann-Schwinger-type integral equation

$$K_{\epsilon'\epsilon} = P \left[\frac{\langle \Phi_{\epsilon'} | V | \Phi_{\epsilon''} \rangle K_{\epsilon''\epsilon}}{\epsilon - \epsilon''} + \langle \Phi_{\epsilon'} | V | \Phi_\epsilon \rangle \right] .$$ (7)

The symbol P represents a principal value integration. The coefficient B_ϵ in Eq. (6) is determined by normalization of the final-state wave function per unit energy,

$$B_\epsilon = \frac{1}{[1 + (\pi K_{\epsilon\epsilon})^2]^{1/2}} .$$ (8)

The matrix elements $\langle \Phi_{\epsilon'} | V | \Phi_\epsilon \rangle$ are residual interaction matrix elements, apart from the parts solely due to the $N-1$ electron core configuration wave functions. For example, the calculated $\langle \Phi_{\epsilon'} | V | \Phi_\epsilon \rangle$ for the Ne atom in the $1s^1 2s^2 2p^6(^2P)\epsilon p (^1P)$ channel are shown in Fig. 3. The integral equation can be recast into an algebraic equation which is readily solved by a matrix inversion. For the details, such as optimal discrete energy mesh and convergence, we refer to Ref. 14. The $K_{\epsilon\epsilon}$ matrix on the energy shell (i.e., the diagonal matrix elements) for the Ne atom in the ^1P channel are shown in Fig. 4. The $K_{\epsilon\epsilon}$ represents a correction $\Delta\mu(\epsilon)$ of the quantum defect $\mu_0(\epsilon)$ which is obtained in the Hartree-Slater potential,
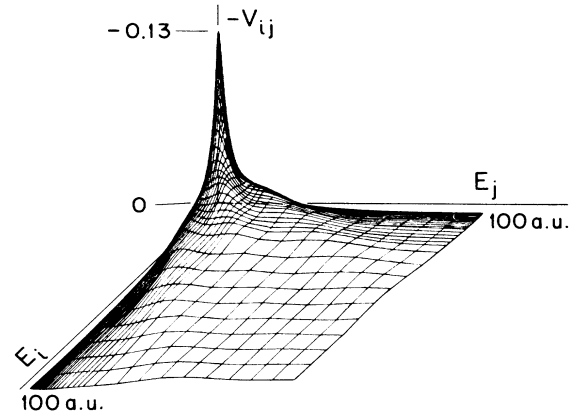

FIG. 3. Residual interaction matrix element $\langle \Phi_{\epsilon'} | V | \Phi_\epsilon \rangle$ for the Ne atom in $1s^1 2s^2 2p^6(^2S)\epsilon p (^1P)$ channel.

$$\Delta\mu(\epsilon) = -\tan^{-1}(\pi K_{\epsilon\epsilon})/\pi .$$ (9)

For the Ne atom in the ^1P channel, $\Delta\mu = 0.17$ at the threshold, indicating that the slow photoelectron feels more attraction due to the dynamical screening effect of the K vacancy produced in the photoionization process.

After obtaining the initial-state and the final-state wave functions, the photoionization cross section can be calculated by first-order perturbation theory,

$$\sigma = (2\pi)^2 \left[\frac{\alpha \omega_K}{3g_I} \right] \sum_\Gamma |\langle \Psi_\epsilon(\Gamma) || r || \Psi_I \rangle|^2 ,$$ (10)

where $\alpha \approx \frac{1}{137}$ is the fine-structure constant, ω_K the photon energy, and g_I the degeneracy of the initial state. For the Ne$^+$ ion, the K-shell photoionization cross section results from the sum of the six final channels. Figure 1 displays the K-shell ratio function of the Ne K shell to the Ne$^+$ K-shell photoionization cross sections. When one includes the configuration interactions in the final state (i.e., mainly the dynamical screening of the K vacancy), the K-shell ratio functions have no oscillations, as
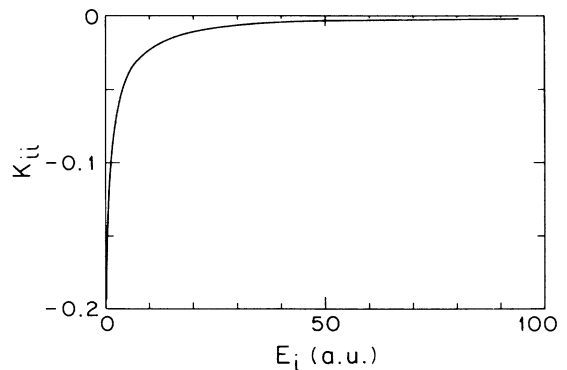

FIG. 4. K matrix on the energy shell for the Ne atom in $1s^1 2s^2 2p^6(^2S)\epsilon p (^1P)$ channel.

shown in Figs. 1(b) and 1(d). The calculated K-shell photoionization cross section for the Ne atom with CI initial-state and CI final-state wave functions is also shown in Fig. 2(a). As we anticipated, the cross section is in good agreement with the experimental data below the shakeup threshold.[23-25]

III. DISCUSSION

First we examine the ratio function of the Ne K shell to the Ne$^+$ K-shell photoionization cross sections. In Fig. 1(a), the K-shell ratio function with Hartree-Slater initial-state and final-state wave functions shows the oscillatory behavior which is associated with a discontinuity in the derivative of the Hartree-Slater potential (with Coulombic Latter tail). If we adopt one-channel CI final-state wave functions, the oscillation disappears as shown in Fig. 1(b). The enhancement of the K-shell ratio function near the Ne$^+$ K-shell threshold is associated with an enhancement of the Ne$^+$ K-shell photoionization cross section near the threshold, reflecting the dynamical screening effect of the K vacancy. In Fig. 1(c), the K-shell ratio function with a CI initial-state and the Hartree-Slater final-state wave functions also has the oscillation. This indicates that the oscillation, due to the discontinuity in the derivative of the Hartree-Slater potential, mainly results from the final-state wave functions. This conclusion is also consistent with the results of model potential calculations.[9] Figure 1(d) displays the K-shell ratio function with both the CI initial-state and the CI final-state wave functions. There is again no oscillation and the enhancement near the Ne$^+$ threshold remains.

Now let us discuss the implication of adopting frozen one-electron orbital wave functions in constructing the $N-1$ electron core configuration wave function. In our present one-channel CI calculations, the major part of the residual interactions due to the K vacancy (i.e., the dynamical screening) has been taken into account but the residual interactions due to more delicate core relaxations such as shakeup and shakeoff have been ignored. According to the variational principle, our one-channel CI

calculations will simulate the K-shell photoionization cross sections below the shakeup threshold. As shown in Fig. 2(a), our one-channel CI cross section agrees with the experimental data below the shakeup threshold. This becomes clearer if we examine the ratios of various Ne K-shell photoionization cross sections with respect to the Hartree-Slater Ne K-shell photoionization cross section as shown in Fig. 2(b). There is an enhancement near threshold due to the dynamical screening effect in our CI result, which is in good agreement with the experimental data.[23-25] As the photon energy increases, the photoelectron will escape faster from the ionic core. At high photon energies above ~60 a.u. as shown in Fig. 2, our one-channel CI photoionization cross section agrees with the experimental K-shell total photoionization cross sections,[23-25] in accord with the physical picture of the sudden approximation. In the photon energy range between the shakeup threshold and the high-energy region, our one-channel CI photoionization cross section is in between the experimental K-shell total photoionization cross sections and the experimental K-shell partial photoionization cross section with the Ne$^+$ ion with a K-shell vacancy. It will require further theoretical multichannel CI calculations to achieve a better understanding of K-shell photoionization in this intermediate photon energy range.

Finally, we would like to conclude by commenting on the K-shell ratio function for Ne and Ne$^+$. Just below the shakeup thresholds, some autoionizing states are expected to exist in rather localized narrow energy regions. The K-shell ratio function is then expected to show Fano-type profiles in these narrow energy regions. Further experimental research is needed, since present experimental measurements of inner-shell photoionization cross sections for atomic ions are very fragmentary.

[1]U. Fano and J. W. Cooper, Rev. Mod. Phys. **40**, 441 (1968).

[2]R. H. Pratt, A. Ron, and H. K. Tseng, Rev. Mod. Phys. **45**, 273 (1973).

[3]D. J. Botto, J. McEnnan, and R. H. Pratt, Phys. Rev. A **18**, 580 (1978).

[4]R. F. Reilman and S. T. Manson, Phys. Rev. A **18**, 2124 (1978).

[5]Xiao-Ling Liang and Jia-Ming Li, Acta Phys. Sin. **34**, 1479 (1985).

[6]Lei Liu, Xiao-Min Tong, and Jia-Ming Li, Acta Phys. Sin. **37**, 1800 (1988).

[7]J. Tulkki and T. Aberg, J. Phys. B **18**, L489 (1985).

[8]M. Ya. Amusia, I. M. Band, V. K. Ivanov, V. A. Kupchenko, and M. B. Trzhaskovskaya, Bull. Acad. Sci. U.S.S.R. **50**, 19 (1986).

[9]Y. Kuang, R. H. Pratt, Y.-J. Wu, J. Stein, I. B. Goldberg, and A. Ron, J. Phys. (Paris) C **9**, 527 (1987).

[10]U. Fano, Phys. Rev. **124**, 1866 (1961).

[11]A. F. Starace, Phys. Rev. A **2**, 118 (1970).

[12]C. D. Lin, Phys. Rev. A **9**, 171 (1974).

[13]L. C. Davis and L. A. Feldkamp, Phys. Rev. B **15**, 2961 (1977).

[14]Yin-Jian Wu and Jia-Ming Li, Acta Phys. Sin. (to be published).

[15]U. Fano and C. M. Lee (Jia-Ming Li), Phys. Rev. Lett. **31**, 1573 (1973).

[16]C. M. Lee (Jia-Ming Li), Phys. Rev. A **10**, 548 (1974).

[17]K. A. Berrington, P. G. Burke, M. LeDourneuf, W. D. Robb, K. T. Taylor, and Vo Ky Lan, Comput. Phys. Commun. **14**, 367 (1977).

[18]C. H. Greene, Phys. Rev. A **28**, 2209 (1983); **32**, 1880 (1985).

[19]M. Ya. Amusia, N. A. Cherepkov, I. Paolin, V. Radojevic, and D. J. Zivanovic, J. Phys. B **10**, 1413 (1977).

[20]W. R. Johnson, C. D. Lin, K. T. Cheng, and C. M. Lee (Jia-Ming Li), Phys. Scr. **21**, 409 (1980).

[21]T. N. Chang, J. Phys. B **8**, 743 (1974).

[22]H. P. Kelley and S. L. Carter, Phys. Scr. **21**, 448 (1980).

[23]F. Wuilleumier and M. O. Krause, Phys. Rev. A **10**, 242 (1974).

[24]F. Wuilleumier, Adv. X-Ray Anal. **16**, 63 (1973).

[25]G. V. Marr and J. B. West, At. Data Nucl. Data Tables **18**, 497 (1976).

[26]F. Herman and S. Skillman, *Atomic Structure Calculations* (Prentice-Hall, Englewood Cliffs, NJ, 1963).

[27]Jia-Ming Li and Zhong-Xin Zhao, Acta Phys. Sin. **30**, 105 (1981).

[28]Zhong-Xi Zhao and Jia-Ming Li, Acta Phys. Sin. **34**, 1496 (1981).